Published in final edited form as:
Nanomedicine. 2012 October ; 8(7): 1190–1199. doi:10.1016/j.nano.2011.12.002.

Quantitative Characterization of the Lipid Encapsulation of Quantum Dots for Biomedical Applications

Justin F. Galloway[1], **Alan Winter**[2], **Kwan Hyi Lee**[1,3], **Jeaho Park**[1], **Charlene Dvoracek**[1], **Peter Devreotes**[4,5], and **Peter C. Searson**[1,5]

[1]Department of Materials Science and Engineering, Johns Hopkins University, Baltimore, Maryland 21218

[2]Department of Biological & Agricultural Engineering, Kansas State University, Manhattan, KS 66506

[4]Department of Cell Biology, Johns Hopkins University, Baltimore, Maryland 21218

[5]Institute for NanoBioTechnology, Johns Hopkins University, Baltimore, Maryland 21218

Abstract

The water solubilization of nanoparticles is key for many applications in biomedicine. Despite the importance of surface functionalization, progress has been largely empirical and very few systematic studies have been performed. Here we report on the water solubilization of QDs using lipid encapsulation. We systematically evaluate the monodispersity, zeta potential, stability, and quantum yield (QY) for QDs encapsulated with single and double acyl chain lipids, pegylated double acyl chain lipids, and single alkyl chain surfactant molecules with charged head groups. We show that charged surfactants and pegylated lipids are important to obtain monodisperse suspensions with high yield and excellent long-term stability.

Keywords

quantum dots; lipids; surface functionalization; biomedicine; solubilization

Introduction

Quantum dots (QDs) possess unique optical properties such as a narrow emission peak, a broad excitation spectrum, and strong resistance to photobleaching.[1, 2, 3] The unique combination of optical properties have led to intense interest, particularly for biomedical applications.[4–8] However, a major challenge in this field has been the transfer of QDs to water.[9, 10]

To whom correspondence should be addressed: searson@jhu.edu.
[3]present address: KIST Biomedical Research Institute, Seoul 136-791, Korea

Appendix A. Supplementary data
Supplementary data associated with this article can be found, in the online version, at XXX

The ability to transfer nanoparticles from organic solvents to water is not trivial. Many approaches for water solubilization have been explored, including: exchanging the native surfactants used in synthesis for thiols or silanes, functionalization with oligomers, dendrimers, saccharides, and polymers such as polyethylene glycol (PEG).[7, 10–12] Other strategies, include functionalization with peptides or proteins,[13] or encapsulation with an inorganic material such as silica.[14, 15] Recently, lipid coating has been explored for water solubilization of a wide range of nanoparticles, including QDs.[16–25]

Despite the critical need for water solubilization and surface functionalization of QDs for biomedical applications, progress has been largely empirical with few systematic studies describing the effectiveness of the different strategies. Indeed, water solubilization is often the roadblock in using QDs in biology and medicine. To evaluate functionalizing schemes for water solubilization there are three key requirements: (1) the QDs should be monodisperse and not aggregate, (2) the QD suspension should be stable for at least several days, and (3) there should be minimum attenuation in the QY. Additionally, the functionalization scheme should allow for incorporation of ligands for conjugation of other molecules, such as antibodies, and should be straightforward, preferably involving commercially available reagents.

In light of these requirements, lipid coating of QDs offer an attractive method for water solubilization for several reasons. First, compared to other methods for water solubilization, lipid coating minimizes the overall size of the surface functionalized QD. Since lipids are typically about 2 nm in length, lipid encapsulation increases the size of the functionalized QD by about 4 nm plus the size of any functional groups. For *in vivo* applications where clearance may be an issue, the ability to minimize the size of the QD can be important. Second, lipid encapsulation is straightforward, taking advantage of the hydrophobic QD surface and the amphiphilic lipids to drive the formation of an outer layer analogous to the outer leaflet in a lipid bilayer or vesicle. Third, many lipids are commercially available, including those with single and double acyl chains, head groups with ligands that can be used for covalent conjugation, and pegylated lipids. This wide range of available lipids and surfactants provides flexibility in designing lipid coatings with multiple components required for specific applications. Finally, lipid coating is a biomimetic approach to water solubilization since lipid coated quantum dots in the size range from 12 – 15 nm are mimics of high density lipoprotein particles in the body.

To enable the widespread use of QDs in a broad range of biomedical applications, it is essential to understand the influence of lipid composition on the monodispersity and stability of QD suspensions in water. Here we report on the quantitative characterization of the physicochemical properties of lipid coated QDs using a combination of absorbance, dynamic light scattering (DLS), zeta potential and QY to assess surface functionalization and stability. We consider a wide range of lipids including single and double acyl chain lipids, the incorporation of charged lipids, and the incorporation of pegylated lipids.

Methods

Chemicals

n-Hexadecylamine (HDA, 90%), trioctylphosphine oxide (TOPO, 90%), trioctylphosphine (TOP, 90%), tributylphosphine (TBP, 97%), stearic acid (SA, 95%), octadecylamine (ODA, 99%) and 1-dodecanethiol (98%) were purchased from Sigma Aldrich (St. Louis, Missouri) and used without further purification. The precursors CdO (99.95%), Se (99.99%), $Cd(C_2H_3O_2)_2{\cdot}2H_2O$ (98%), $Zn(C_{18}H_{35}O_2)_2$ (Tech Grade), and bis(trimethylsilyl) sulfide ($(TMS)_2S$, purum) were purchased from Sigma Aldrich. MHPC, DSPE-PEG2k, 1,2-dipalmitoyl-sn-glycero-3-phosphoethanolamine (DPPE), 1,2-dipalmitoyl-*sn*-glycero-3-

phosphoethanolamine-N-(lauroyl) (sodium salt) (DPPE-COOH), 1,2-dipalmitoyl-sn-glycero-3-phosphoethanolamine-N-(lauroylamine) (DPPE-NH_2) were purchased from Avanti Polar Lipids (Alabaster, Alabama). Hexane, methanol, chloroform and ethanol were HPLC grade.

Synthesis of CdSe/(Cd,Zn)S QDs

CdSe cores were synthesized from CdO and Se in TOPO and HDA (Supporting Information). The average QD diameter, determined from analysis of TEM images, was 6.0 nm corresponding to a peak photoluminescence of 600 nm.[26] The CdSe QDs were passivated with a (Cd,Zn)S shell (Supporting Information). The concentration of the QDs in chloroform was determined from the absorbance at 350 nm using Beer's Law ($A = \varepsilon lc$) and an extinction coefficient $\varepsilon = 1.438 \times 10^{26} \times r^3$ ($cm^2\ mol^{-1}$).[27] The average thickness of the shell, determined from analysis of TEM images, was 0.95 nm resulting in an overall core/shell diameter of 7.9 nm.[28]

CdSe(Cd,Zn)S thiolation

The native HDA/ODA ligands were displaced by incubating the core/shell QDs in chloroform with dodecanethiol (DDT) (Supporting Information).

Lipid coating

The lipids were dissolved in chloroform and mixed with a suspension of QDs in chloroform. The mixture of QDs and lipids in chloroform was then added dropwise to water and sonicated prior to raising the temperature to drive off the chloroform (Supporting Information).

Characterization

Absorbance spectra were obtained using a Varian Cary 50 UV/Vis Spectrophotometer (Agilent Technologies, Santa Clara, CA). For CdSe(Cd,Zn)S QDs suspended in chloroform it was necessary to dilute the starting solution. Typically, 2 μL QD suspension was added to 700 μL chloroform in a quartz cuvette. For water solubilized QDs, dilution was not necessary and the entire sample was used for absorbance measurements.

The effectiveness of water solubilization was determined by the fraction of QDs recovered after water solubilization and filtration. The fraction recovered is defined as the number moles of QDs recovered after water solubilization and filtration normalized to the number of moles of QDs in chloroform prior to water solubilization.

The stability of the QD suspensions was determined at different times after water solubilization using absorbance measurements. The QD suspension was filtered through a 200 nm, PTFE 13 mm diameter syringe filter prior to each measurement. The fraction of QDs recovered was determined as described above. The QY was obtained using a C9920-02 Quantum Yield Measurement System (Hamamatsu, Japan) (Supplemental Information). Particle size distributions and zeta potential were obtained using a Nano Zetasizer (Malvern, Worcestershire, UK) (Supplemental Information). Error bars represent the standard error. Student's t-tests with unpaired variance were used for statistical comparisons.

RESULTS

Quantum dots were encapsulated with an outer leaflet consisting of lipids with either single or double acyl chains and surfactant molecules. A summary of the lipid compositions and results is provided in Table 1. SA and ODA are surfactant molecules with C18 alkyl chains and terminal carboxylic acid or amine groups, respectively, that can introduce charge into

the lipid encapsulation layer depending on the pH. MHPC is a zwitterionic phospholipid with a single C14 acyl chain. DSPE and DPPE are zwitterionic phospholipids with double C18 or C16 acyl chains, respectively. In addition, we studied water solubilization with modified DPPE lipids incorporating charged carboxylic acid or amine groups on a short C11 spacer (DPPE-COOH, DPPE-NH_2), and incorporating a 2000 kDa polyethylene glycol group attached to the head group of the phospholipid (DSPE-PEG2k). The inner leaflet was formed from the native surfactants TOPO and HDA used in the synthesis, or DDT after surfactant exchange.

Figures 1 and 2 show results for lipid functionalization of QDs with an MHPC/SA or MHPC/ODA outer leaftlet and a TOPO/HDA inner leaflet. Each figure shows absorbance spectra before and after water solubilization, the fraction of QDs recovered after water solubilization, size distributions, zeta potential as a function of SA or ODA concentration, and the stability versus time. The fraction of QDs recovered, determined from the absorbance at 350 nm, is a measure of the effectiveness of water solubilization since any aggregates larger then 200 nm are removed in the filtration step. Similar results were obtained for QDs with a DDT inner leaflet. Figure 3 shows the quantum yield versus SA and ODA concentration for MHPC/SA and MHPC/ODA functionalized QDs with either TOPO/HDA or DDT inner leaflet.

Figures 4a and 4b show the fraction recovered and zeta potential for lipid functionalization with 80 mol% MHPC, 20 – × mol% DPPE, and × mol% DPPE-COOH or DPPE-NH_2. Figure 4c shows the time dependence of the fraction recovered for QDs functionalized with 80 mol% MHPC and 20 mol% DPPE-COOH or DPPE-NH_2.

Figures 5a – 5c show the fraction recovered, size distributions, and zeta potential for QDs functionalized with MHPC and DSPE-PEG2k. Figure 5d shows the fraction recovered versus time for QDs functionalized with 80 mol% MHPC and 20 mol% DSPE-PEG2k. Figures 6a – 6e show the fraction recovered, zeta potential, size distributions (10 mol% and 20 mol% DSPE-PEG2k), and quantum yield for QDs with a DDT inner leaflet and an ODA/MHPC/DSPE-PEG2k outer leaflet (30 mol% ODA) versus the concentration of DSPE-PEG2k. Figure 6f shows the fraction recovered versus DSPE-PEG2k concentration after incubation in 100 mM phosphate buffer for 1 h.

DISCUSSION

SA and MHPC outer leaflet and HDA/TOPO inner leaflet

Figure 1a shows a schematic illustration of lipid functionalization of QDs with MHPC and SA on unthiolated QDs. The absorbance spectra for the HDA/TOPO modified QDs in chloroform and the lipid coated QDs in water (Figure 1b) show the same features with an absorbance onset at about 655 nm, a first exciton peak at 600 nm, and a second exciton peak at about 500 nm. Figure 1c shows the fraction of QDs recovered after water solubilization and filtration versus the mole fraction of SA ($c_{SA}/(c_{SA} + c_{MHPC})$) in bulk solution. The fraction recovered increases from about 6% (Figure 1c) for QDs with an outer leaflet of 100% MHPC, to a maximum of more than 60% recovered at higher SA concentrations. These results indicate that the single acyl chain phospholipid alone is not particularly effective in minimizing aggregation and sedimentation, but the progressive addition of SA increases the colloidal stability in water.

Size distributions for QDs with 20 mol% and 30 mol% SA (Figure 1d) show a single peak with average sizes of 13.6 ± 1.0 nm and 15.2 ± 1.2 nm, respectively. The average diameter of the CdSe/(Cd,Zn)S QDs is about 8 nm. Taking the thickness of the HDA/TOPO inner leaflet as 1 nm and the MHPC/SA outer leaflet as 2 nm, the diameter of a single

functionalized QD is expected to be about 14 nm, in excellent agreement with the values obtained from the size distributions in water. These results confirm that a lipid monolayer is formed on the surface of the HDA/TOPO modified QDs and that the QDs are monodisperse.

The initial increase in fraction recovered with SA concentration indicates that the incorporation of negative charge into the outer leaflet of the lipid layer increases the stability of the QDs in water. The zeta potential for QDs functionalized with 100% MHPC is in the range 1 – 10 mV, but decreases linearly with increasing SA concentration in bulk solution (Figure 1e). Since the QDs are suspended in distilled water we expect that only a fraction of the carboxylic acid groups on the SA are deprotonated. The incorporation of negative charge onto the QD surface can be determined from the zeta potential. For a spherical particle, the zeta potential ζ is given by:[29]

$$\zeta = \frac{q}{4\pi\varepsilon\varepsilon_0 r} - \frac{q}{4\pi\varepsilon\varepsilon_0 (r + \lambda^{-1})} \quad (1)$$

where r is the particle radius, q is the charge on the particle (C), ε is the relative permittivity, ε_0 is permittivity of free space (8.854×10^{-14} F cm^{-1}), and λ^{-1} is the Debye length. λ is given by:

$$\lambda = \left(\frac{2000 e^2 N_A I}{\varepsilon\varepsilon_0 kT} \right)^{1/2} \quad (2)$$

where e is the charge on the electron, N_A is Avogadro's number, I is the ionic strength (½Σ $z_i^2 c_i$), k is the Boltzmann constant, and T is temperature.

The surface concentration of charged lipids on the QDs can be calculated from the zeta potential using eq. (1). To calculate the Debye length, the ionic strength I was related to the conductivity κ using the empirical expression derived for low conductivity (<10^{-3} S cm^{-1}) solutions (Supporting Information):[30]

$$I = 12\kappa - 0.0002 \quad (3)$$

The conductivities of the QD suspensions varied from about 58×10^{-6} S cm^{-1} to about 84×10^{-6} S cm^{-1} and were independent of lipid concentration. The solid line in Figure 1e shows a least squares fit to eq. (1) using r =7 nm, ε =80, and q as an adjustable parameter. The Debye length, calculated from the conductivity measured for each sample, ranged from 10.9 to 12.4 nm. From the fit we determine that 4.6% of the SA groups are charged (deprotonated). The excellent agreement over the whole concentration range indicates that incorporation of SA is related to the concentration in the bulk solution and the pK_a and is not influenced by other effects.

The number of charged SA groups on a QD can be calculated in the following way. We take the footprint of SA as 0.2 nm^2 [31] and the footprint for MHPC as 0.50 nm^2.[32] For a diameter of 12 nm, corresponding to the midpoint of the outer leaflet, we estimate a total of about 865 lipids on the surface (see Supplemental Information for details), and hence 12 charged SA molecules at a concentration of 30 mol% SA.

As shown in Figure 1e, the zeta potential decreases linearly up to 50 mol% SA, corresponding to about 20 charged SA groups. We can estimate the maximum number of charged groups that can be accommodated before electrostatic repulsion becomes significant in the following way. The interaction energy E(r) between two point charges at separation r is given by $E(r) = q_1 q_2/(4p\varepsilon\varepsilon_0 r)$. If we take the screening length as the distance at which the energy falls to 1/e(kT), then the screening length for two unit charges in water (ε = 80) is

about 2 nm (Supporting Information). Taking a diameter of 12 nm, the maximum number of charged lipids per QD is estimated to be 28, suggesting that the value of 20 obtained at 50 mol% SA is close to the maximum that can be accommodated.

The long-term stability of the QD suspensions was determined by measuring the fraction of QDs recovered after water solubilization and filtration as a function of time. Figure 1f shows the fraction recovered for an outer leaflet with 25 mol% SA versus time, indicating that after water solubilization, the suspension remains stable with little aggregation or precipitation for at least 2000 h (~3 months). There is a strong correlation between zeta potential and fraction recovered (Supporting Information) indicting that charge incorporation plays a significant role in the stability and monodispersity of lipid coated QDs.

ODA and MHPC outer leaflet and HDA/TOPO inner leaflet

Having characterized the functionalization of QDs with incorporation of negative charge (SA), we next studied the incorporation of positive charge by using ODA (Figure 2a). Figure 2b shows the absorbance spectra before and after water solubilization and filtration for QDs with 20 mol% ODA indicating a relatively small loss due to precipitation and aggregation. Figure 2c shows that incorporating positive charge into the outer leaflet dramatically increases stability. The fraction recovered increases linearly with ODA concentration reaching a maximum of nearly 80% recovered for ODA concentrations greater than 15 mol %. Comparison of Figures 1c and 2c suggests that ODA is more effective than SA in producing stable, monodisperse QD suspensions in water.

Size distributions for QDs with 20 and 30 mol% ODA (Figure 2d) revealed average diameters of 15.0 ± 1.5 nm and 15.2 ± 0.8 nm, respectively. These values are in excellent agreement with the values obtained for SA/MHPC functionalized QDs, and confirm that the QDs are monodisperse.

The zeta potential for the ODA/MHPC QDs is shown in Figure 2e. The incorporation of positive charge results in an increase in the zeta potential and stability. The solid line corresponds to a least squares fit to eq. (1) with 5.2% charged ODA molecules on the surface. The long-term stability of QDs with 25 mol% ODA and MHPC (Figure 4f) shows that the fraction recovered remains constant for at least 3 months.

SA/MHPC or ODA/MHPC outer leaflet and dodecanethiol inner leaflet

The preceding work examined the influence of the outer leaflet composition on the physicochemical properties of QDs in water. In these experiments the inner leaflet is formed by HDA and TOPO that weakly adsorb to the QD surface during synthesis. To determine whether alkanethiols could increase the stability, we characterized QDs where the HDA/TOPO surface layer was displaced by 1-dodecanethiol. Thiolated QDs were then water solubilized using the same outer leaflet as unthiolated QDs and assessed using the same quantitative measurements. For both SA/MHPC and ODA/MHPC outer leaflets, there was no significant difference in the fraction recovered, monodispersity, zeta potential, or long-term stability with TOPO/HDA or DDT as the inner leaflet (Supporting Information).

Although there was no significant difference in physicochemical properties of QDs with a TOPO/HDA or DDT inner leaflet, the QY was significantly higher for QDs with a DDT inner leaflet (see Figure 3). For an SA/MHPC outer leaflet, the QY is weakly dependent on the SA concentration, however, the average value increases from 20.9 ± 1.9% before thiolation to 32.2 ± 2.5% after thiolation. The QY for the ODA/MHPC functionalized QDs increased from 29.7 ± 1.1% before thiolation to 46.9 ± 3.8% after thiolation with a maximum of 62%. Thiolation has been reported to passivate surface states and increase the photoluminescence.[33] As seen from the absorbance spectra (Supporting Information),

thiolation strongly influences the electronic coupling of the inner leaflet, and hence it is not surprising that the quantum yield is also increased significantly.

DSPE/MHPC or DPPE/MHPC outer leaflet and TOPO/HDA inner leaflet

To compare encapsulation with single and double acyl chains, we water solubilized QDs with MHPC and the zwitterionic phospholipid DSPE. The fraction of QDs recovered after water solubilization was 20 – 30% up to a bulk DSPE concentration of 20 mol%, but decreased at higher concentrations (Supporting Information). The fraction recovered for the shorter palmitoyl phospholipid DPPE was found to be similar to DSPE. The zeta potential for QDs with DSPE and DPPE in the outer leaflet was in the range from 5 – 15 mV, only slightly higher tha n the range observed for QDs functionalized with 100 mol% MHPC. This result is expected given that both DSPE and DPPE are zwitterionic. The size distribution for QDs with 20 mol% DSPE showed a single peak with an average particle size of 16.7 ± 2.1 nm, slightly higher than for SA/MHPC or ODA/MHPC functionalization, presumably reflecting the slightly longer double acyl chain phospholipid. The QDs with 20 mol% DSPE remain stable for 3 – 4 days, significantly lower than the stability of the SA/MHPC or ODA/MHPC modified QDs. Comparable stability results were observed for DPPE. These results suggest that the incorporation of more than 20 mol% of a double acyl chain lipid decreases monodispersity and stability. This effect is ascribed to the difficulty in accommodating the high curvature of the quantum dots with the double acyl chain lipids. The average head group spacing is expected to increase with increasing curvature resulting in progressive deviation from a parallel alignment of lipids and increasing permeability to solvent molecules.

DPPE-COOH/MHPC or DPPE-NH_2/MHPC outer leaflet and TOPO/HDA inner leaflet

The stability of QDs encapsulated only with single or double acyl chain lipids (MHPC, MHPC/DSPE, or MHPC/DPPE) was not as good as for QDs incorporating charged lipids in the outer leaflet. Therefore, we characterized the physicochemical properties of QDs with an outer leaflet incorporating DPPE with a terminal amine (DPPE-NH_2), or carboxylic acid (DPPE-COOH) group at the end of a C11 spacer. In these experiments, the concentration of the single acyl chain MHPC lipid was fixed at 80 mol%. The fraction of QDs recovered (Figure 4a) is relatively independent of DPPE-NH_2 concentration, but increases slightly with DPPE-COOH concentration, reaching a maximum of 43% recovered at 20 mol% DPPE-COOH. Thiolation of the QDs prior to formation of the outer leaflet did not significantly influence the fraction of QDs recovered after water solubilization. This result suggests that the addition of negatively charged, double acyl chain phospholipids only moderately improves the fraction of QDs recovered, and no improvement is seen with positively charged lipids.

The zeta potential for QDs functionalized with MHPC and DPPE-COOH is shown in Figure 4b. Increasing the concentration of DPPE-COOH results in a progressive decrease in the surface charge, as can be seen from the negative slope. From the fit, using a QD radius of 7.5 nm to reflect the larger hydrodynamic radius, we determine that 12.3% of the DPPE-COOH molecules in the surface layer are charged (deprotonated). This result indicates that incorporation of phospholipids with charged groups on short spacers is more effective than single alkyl chain surfactants at introducing surface charge, however, the single alkyl chain surfactant is more effective in producing a stable suspension in water.

In contrast, the zeta potential for QDs functionalized with DPPE-NH_2 was independent of concentration. This is surprising since it indicates that either the DPPE-NH_2 is not incorporated into the outer leaflet, or that the DPPE-NH_2 is unprotonated and hence neutral. The fraction of QDs recovered is plotted versus time in Figure 4c for 20 mol% DPPE-NH_2

and 20 mol% DPPE-COOH. The QDs remain stable for about 50 h, however, the fraction recovered remains significantly higher for those functionalized with DPPE-COOH due to the large negative zeta potential. These results suggest that charged, double acyl phospholipids are not as effective as single alkyl chain lipids for water solubilization.

DSPE-PEG2k/MHPC outer leaflet and TOPO/HDA inner leaflet

Pegylated lipids are often used for nanoparticle functionalization. Figure 5a shows the fraction of QDs recovered after water solubilization with MHPC/DSPE-PEG2k, illustrating that the fraction recovered increases to around 40% for 20 – 50 mol% DSPE-PEG2k. The average size of QDs functionalized with 20 mol% DSPE-PEG2k (Figure 5b) is 20.5 ± 0.9 nm. This is about 4 nm larger than the value of 16.7 nm measured for QDs functionalized with 20 mol% DSPE, indicating that the polyethylene glycol groups increase the average hydrodynamic size by about 4 nm. The radius of gyration of a polymer is given by:

$$r_g = \frac{1}{\sqrt{6}} a \sqrt{N} \quad (5)$$

where a is the persistence length and N is the number of monomers. Taking a =0.35 nm for the C-O-C monomer unit,[34] we obtain a diameter of 2 nm for PEG2k. Thus we expect an increase in diameter of about 4 nm for a QD coated with a PEG2k lipid. For concentrations less than 20 mol% DSPE-PEG2k, the fraction of QDs recovered and particle size distributions were not reproducible. In contrast, at concentrations =20 mol% DSPE-PEG2k, the results were reproducible with a fraction recovered of about 40% and an average particle size of about 21 nm (Figure 5).

The addition of DSPE-PEG2k results in a decrease in the zeta potential from 1.6 ± 0.2 mV to approximately −9 mV for 10 – 50 mol% DSPE-PEG2k (Figure 5c). Figure 5d demonstrates that QDs with 20 mol% DSPE-PEG have good stability over about 500 h, with a fraction of QDs recovered maintained above 30%. In summary, the incorporation of pegylated lipids results in a negative zeta potential that is sufficiently large to produce monodisperse suspensions with moderately high fraction recovered after water solubilization.

ODA/MHPC|DSPE-PEG2k outer leaflet and DDT inner leaflet

To introduce charged groups into QDs functionalized with double acyl chain phospholipids, we studied QDs functionalized with ODA/MHPC/DSPE-PEG2k (Figure 6a). For these experiments the inner leaflet was DDT and the ODA concentration in the outer leaflet was fixed at 30 mol%. The ODA concentration was selected due to the high fraction recovered and high quantum yield (Figure 3b) observed for ODA/MHPC functionalized QDs. The fraction of QDs recovered after water solubilization (Figure 6b) is very high but surprisingly decreases progressively with increasing DSPE-PEG2k concentration. In comparison to QDs functionalized with MHPC/DSPE-PEG2k (Figure 5), the presence of the ODA increases the fraction recovered dramatically, at least for lower DSPE-PEG2k concentrations. In contrast, the presence of ODA does not improve the stability, as measured by the fraction recovered, at higher DSPE-PEG2k concentrations. The fraction recovered for ODA/DSPE-PEG2k/MHPC at 20 mol% was about 25%, consistent with DSPE-PEG2k/MHPC where the fraction recovered was about 35% at 20 mol%. This effect is likely due to PEG groups screening ODA at higher at DSPE-PEG2k, as can be seen from the progressive decrease in magnitude of the zeta potential (Figure 6c).

The zeta potential for QDs with 30 mol% ODA and different concentrations of DSPE-PEG2k (Figure 6c) decreased from 37.3 ± 0.3 mV to 22.3 ± 0.3 mV at 20 mol% DSPE-

PEG2k. This decrease is similar to the decrease in fraction recovered and supports the hypothesis that increasing the mole fraction of DSPE-PEG2k progressively decreases the fraction of charged ODA groups in the lipid layer.

The size distributions for QDs with 10 mol% and 20 mol% DSPE-PEG2k show that the particles are monodisperse with no aggregation. The average diameters of 16.0 ± 0.5 nm and 17.8 ± 0.6 nm, respectively, are smaller than MHPC/DSPE-PEG2K but larger than MHPC/ODA. The QY was 60%, independent of DSPE-PEG2k concentration (Figure 6e). A similarly high QY was observed for thiolated QDs with ODA/MHPC (Figure 3b), suggesting that thiolation and the incorporation of a positively charged lipid both contribute to the increase.

An advantage of PEG lipids for functionalization of nanocrystals is the additional stability provided in high ionic strength buffers. The fraction of water-soluble QDs recovered after suspending in 100 mM phosphate buffer is 60 – 70% at low DSPE-PEG2k concentrations (Figure 6f), but increases significantly at higher DSPE-PEG2k concentrations. These results demonstrate that QDs functionalized with ODA/MHPC/DSPE-PEG2k remain monodisperse and maintain good stability even in buffer.

We have systematically investigated the physicochemical properties of QDs functionalized with a range of commercially available single and double acyl chain lipids, pegylated double acyl chain lipids, and single alkyl chain surfactant molecules with charged head groups and demonstrate that monodisperse suspensions with a very high fraction of QDs recovered after water solubilization and excellent stability can be achieved. High stability and monodispersity can be achieved with a single acyl chain lipid combined with a charged surfactant. The addition of more than 20 mol% of a double acyl chain zwitterionic lipid to a single acyl chain lipid encapsulation layer results in a decrease in stability due to the high curvature. The addition of a pegylated double acyl chain lipids results in a small negative zeta potential and moderate stability. A combination of single acyl chain lipids, double acyl chain pegylated lipids, and charged surfactants results in excellent stability in water or buffer. Replacing the native TOPO/HDA surfactants with 1-dodecanethiol does not significantly influence the monodispersity and stability of the colloidal suspensions but dramatically increases the QY in water.

Supplementary Material

Refer to Web version on PubMed Central for supplementary material.

Acknowledgments

The authors gratefully acknowledge the support from NIH (U54CA151838) and NSF (CHE-0905869). JFG acknowledges support from the NSF-IGERT graduate training program. AW acknowledges support from the INBT REU program.

References

1. Alivisatos AP. Semiconductor clusters, nanocrystals, and quantum dots. Science. 1996; 271(5251): 933–937.
2. Murray CB, Kagan CR, Bawendi MG. Synthesis and characterization of monodisperse nanocrystals and close-packed nanocrystal assemblies. Annual Review of Materials Science. 2000; 30:545–610.
3. Brus LE. Electron Electron and Electron-Hole Interactions in Small Semiconductor Crystallites - the Size Dependence of the Lowest Excited Electronic State. Journal of Chemical Physics. 1984; 80(9): 4403–4409.

4. Alivisatos P. The use of nanocrystals in biological detection. Nature Biotechnology. 2004; 22:47–52.
5. Resch-Genger U, Grabolle M, Cavaliere-Jaricot S, Nitschke R, Nann T. Quantum dots versus organic dyes as fluorescent labels. Nature Methods. 2008; 5(9):763–775. [PubMed: 18756197]
6. Smith BR, Cheng Z, De A, Koh AL, Sinclair R, Gambhir SS. Real-time intravital imaging of RGD-quantum dot binding to luminal endothelium in mouse tumor neovasculature. Nano Letters. 2008; 8(9):2599–2606. [PubMed: 18386933]
7. Michalet X, Pinaud FF, Bentolila LA, Tsay JM, Doose S, Li JJ, et al. Quantum dots for live cells, in vivo imaging, and diagnostics. Science. 2005; 307(5709):538–544. [PubMed: 15681376]
8. Gao XH, Cui YY, Levenson RM, Chung LWK, Nie SM. In vivo cancer targeting and imaging with semiconductor quantum dots. Nature Biotechnology. 2004; 22(8):969–976.
9. Medintz IL, Uyeda HT, Goldman ER, Mattoussi H. Quantum dot bioconjugates for imaging, labelling and sensing. Nat Mater. 2005; 4(6):435–446. [PubMed: 15928695]
10. Louie A. Multimodality Imaging Probes: Design and Challenges. Chemical Reviews. 2010; 110(5):3146–3195. [PubMed: 20225900]
11. Mattoussi H, Mauro JM, Goldman ER, Anderson GP, Sundar VC, Mikulec FV, et al. Self-assembly of CdSe-ZnS quantum dot bioconjugates using an engineered recombinant protein. Journal of the American Chemical Society. 2000; 122(49):12142–12150.
12. Chan WCW, Nie SM. Quantum dot bioconjugates for ultrasensitive nonisotopic detection. Science. 1998; 281(5385):2016–2018. [PubMed: 9748158]
13. Cai WB, Chen XY. Preparation of peptide-conjugated quantum dots for tumor vasculature-targeted imaging. Nature Protocols. 2008; 3(1):89–96.
14. Fu A, Gu W, Boussert B, Koski K, Gerion D, Manna L, et al. Semiconductor Quantum Rods as Single Molecule Fluorescent Biological Labels. Nano Letters. 2006; 7(1):179–182. [PubMed: 17212460]
15. Zhang JZ, Wolcott A, Gerion D, Visconte M, Sun J, Schwartzberg A, et al. Silica-coated CdTe quantum dots functionalized with thiols for bioconjugation to IgG proteins. J Phys Chem B. 2006; 110(11):5779–5789. [PubMed: 16539525]
16. Dubertret B, Skourides P, Norris DJ, Noireaux V, Brivanlou AH, Libchaber A. In vivo imaging of quantum dots encapsulated in phospholipid micelles. Science. 2002; 298(5599):1759–1762. [PubMed: 12459582]
17. van Schooneveld MM, Vucic E, Koole R, Zhou Y, Stocks J, Cormode DP, et al. Improved biocompatibility and pharmacokinetics of silica nanoparticles by means of a lipid coating: A multimodality investigation. Nano Letters. 2008; 8(8):2517–2525. [PubMed: 18624389]
18. Cormode DP, Skajaa T, van Schooneveld MM, Koole R, Jarzyna P, Lobatto ME, et al. Nanocrystal Core High-Density Lipoproteins: A Multimodality Contrast Agent Platform. Nano Letters. 2008; 8(11):3715–3723. [PubMed: 18939808]
19. Koole R, van Schooneveld MM, Hilhorst J, Castermans K, Cormode DP, Strijkers GJ, et al. Paramagnetic Lipid-Coated Silica Nanoparticles with a Fluorescent Quantum Dot Core: A New Contrast Agent Platform for Multimodality Imaging. Bioconjugate Chemistry. 2008; 19(12):2471–2479. [PubMed: 19035793]
20. Mulder WJM, Koole R, Brandwijk RJ, Storm G, Chin PTK, Strijkers GJ, et al. Quantum dots with a paramagnetic coating as a bimodal molecular imaging probe. Nano Letters. 2006; 6(1):1–6. [PubMed: 16402777]
21. Mulder WJM, Strijkers GJ, van Tilborg GAF, Cormode DP, Fayad ZA, Nicolay K. Nanoparticulate Assemblies of Amphiphiles and Diagnostically Active Materials for Multimodality Imaging. Accounts of Chemical Research. 2009; 42(7):904–914. [PubMed: 19435319]
22. Carion O, Mahler B, Pons T, Dubertret B. Synthesis, encapsulation, purification and coupling of single quantum dots in phospholipid micelles for their use in cellular and in vivo imaging. Nature Protocols. 2007; 2(10):2383–2390.
23. Pons T, Uyeda HT, Medintz IL, Mattoussi H. Hydrodynamic dimensions, electrophoretic mobility, and stability of hydrophilic quantum dots. J Phys Chem B. 2006; 110(41):20308–20316. [PubMed: 17034212]

24. Al-Jamal WT, Al-Jamal KT, Tian B, Lacerda L, Bornans PH, Frederik PM, et al. Lipid-quanturn dot bilayer vesicles enhance tumor cell uptake and retention in vitro and in vivo. Acs Nano. 2008; 2(3):408–418. [PubMed: 19206564]
25. Depalo N, Mallardi A, Comparelli R, Striccoli M, Agostiano A, Curri ML. Luminescent nanocrystals in phospholipid micelles for bioconjugation: An optical and structural investigation. J Colloid Interf Sci. 2008; 325(2):558–566.
26. Park J, Lee KH, Galloway JF, Searson PC. Synthesis of Cadmium Selenide Quantum Dots from a Non-Coordinating Solvent: Growth Kinetics and Particle Size Distribution. J Phys Chem C. 2008; 112(46):17849–17854.
27. Leatherdale CA, Woo WK, Mikulec FV, Bawendi MG. On the absorption cross section of CdSe nanocrystal quantum dots. J Phys Chem B. 2002; 106(31):7619–7622.
28. Galloway JF, Park J, Lee KH, Wirtz D, Searson PC. Exploiting Nucleation and Growth in the Synthesis and Electrical Passivation of CdSe Quantum Dots. Science of Advanced Materials. 2009; 1(1):1–8.
29. Hiemenz, RC.; Rajagopalan, R. Principles of Colloid and Surface Chemistry. 3 ed.. New York: Taylor & Francis; 1997.
30. Alva AK, Sumner ME, Miller WP. Relationship between ionic-strength and electrical conductivity for soil solutions. Soil Sci. 1991; 152(4):239–242.
31. Rontu N, Vaida V. Miscibility of perfluorododecanoic acid with organic acids at the air-water interface. J Phys Chem C. 2007; 111(27):9975–9980.
32. Hauser H, Pascher I, Pearson RH, Sundell S. Preferred Conformation and Molecular Packing of Phosphatidylethanolamine and Phosphatidylcholine. Biochim Biophys Acta. 1981; 650(1):21–51. [PubMed: 7020761]
33. Sargent EH, Barkhouse DAR, Pattantyus-Abraham AG, Levina L. Thiols Passivate Recombination Centers in Colloidal Quantum Dots Leading to Enhanced Photovoltaic Device Efficiency. Acs Nano. 2008; 2(11):2356–2362. [PubMed: 19206403]
34. Movileanu L, Bayley H. Partitioning of a polymer into a nanoscopic protein pore obeys a simple scaling law. Proceedings of the National Academy of Sciences of the United States of America. 2001; 98(18):10137–10141. [PubMed: 11504913]
35. Lin J, Szymanski J, Searson PC, Hristova K. Effect of a Polymer Cushion on the Electrical Properties and Stability of Surface-Supported Lipid Bilayers. Langmuir. 2010; 26(5):3544–3548. [PubMed: 20175577]
36. Kuhl TL, Leckband DE, Lasic DD, Israelachvili JN. Modulation of Interaction Forces between Bilayers Exposing Short-Chained Ethylene-Oxide Headgroups. Biophysical Journal. 1994; 66(5): 1479–1488. [PubMed: 8061197]

Abbreviations

QDs	Quantum Dots
DSPE-PEG2k	1,2-distearoyl-sn-glycero-3-phosphoethanolamine-N-[methoxy (polyethylene glycol)-2000] (ammonium salt)
DPPE-PEG2k	1,2-dipalmitoyl-sn-glycero-3-phosphoethanolamine-N-[methoxy(polyethylene glycol)-2000] (ammonium salt)
DMPE	1,2-dimyristoyl-sn-glycero-3-phosphoethanolamine
MHPC	1-myristoyl-2-hydroxy-sn-glycero-3-phosphocholine
DLS	dynamic light scattering
DDT	1-dodecanethiol
SA	stearic acid
ODA	octadecylamine

DSPE	1,2-distearoyl-sn-glycero-3-phosphoethanolamine
DPPE	1,2-dipalmitoyl-sn-glycero-3-phosphoethanolamine
DPPE-COOH	1,2-dipalmitoyl-*sn*-glycero-3-phosphoethanolamine-N-(lauroyl) (sodium salt)
DPPE-NH_2	1,2-dipalmitoyl-sn-glycero-3-phosphoethanolamine-N-(lauroylamine)
TOPO	trioctylphosphine oxide
HDA	1-hexadecylamine

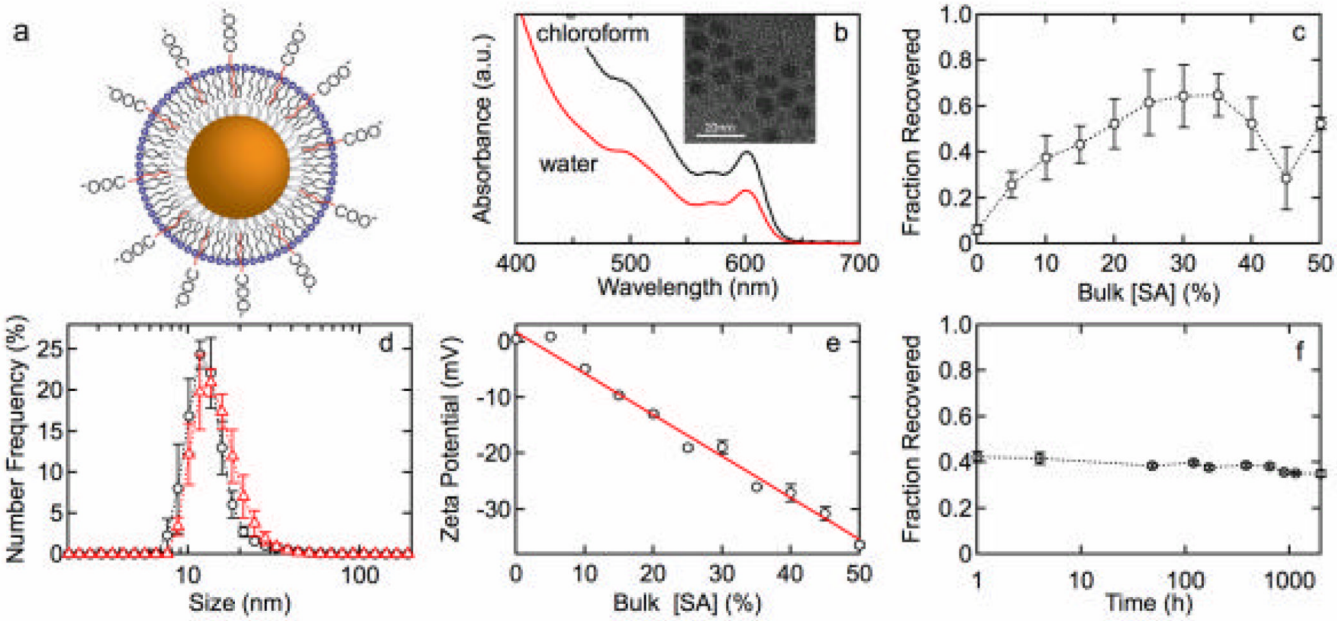

Figure 1.

(a) QD lipid functionalization scheme: TOPO/HDA inner leaflet and SA/MHPC outer leaflet. (b) Absorbance spectrum for QDs with 20 mol% SA before and after water solubilization. (c) Fraction of QDs recovered versus SA concentration 30 min after water solubilization. (d) Size distributions for QDs with (o) 20 mol% and (?) 30 mol% SA with average sizes of 13.6 ± 1.0 nm and 15.2 ± 1.2 nm, respectively. (e) Zeta potential versus mole fraction of SA. The solid line represents a least squares fit that corresponds to 4.6% charged (deprotonated) SA groups. (f) The stability of QDs functionalized with 25 mol% SA versus time.

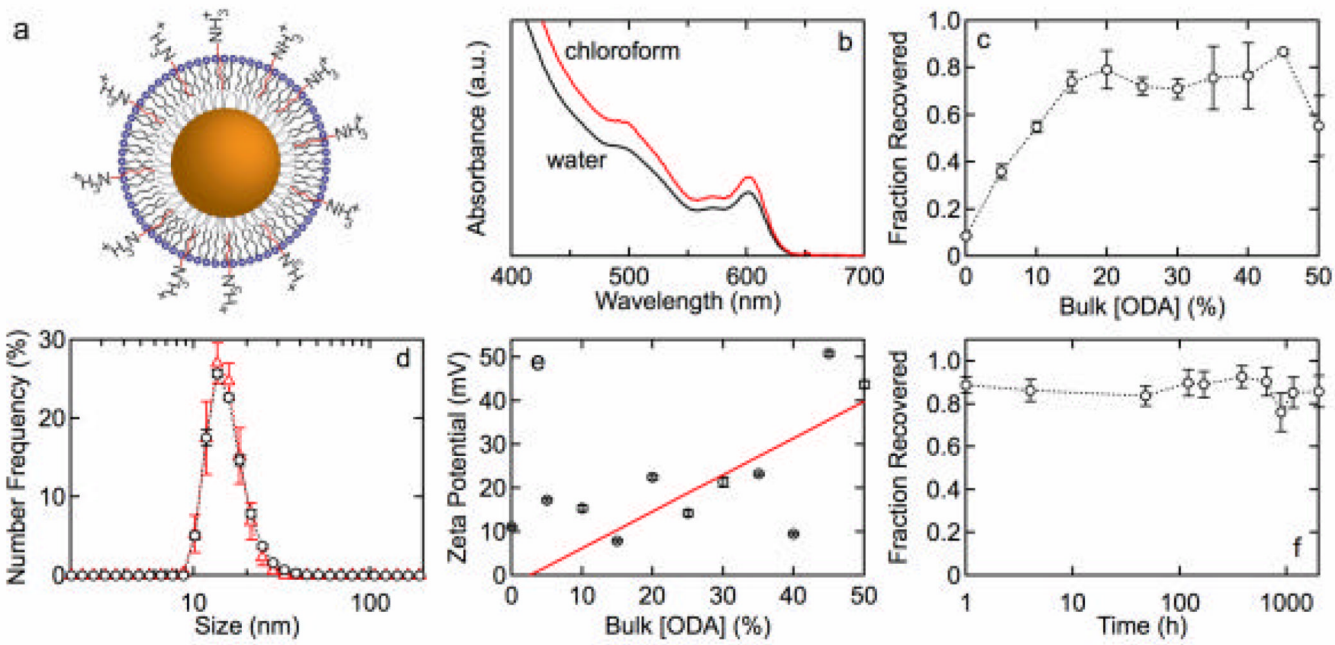

Figure 2.

(a) QD lipid functionalization scheme: TOPO/HDA inner leaflet and ODA/MHPC outer leaflet. (b) Absorbance spectrum for QDs with 20 mol% ODA before and after water solubilization. (c) Fraction of QDs recovered versus ODA concentration 30 min after water solubilization. (d) Size distributions for QDs with (o) 20 mol% and (?) 30 mol% ODA with average sizes of 15.0 ± 1.5 nm and 15.2 ± 0.8 nm, respectively. (e) Zeta potential versus mole fraction of ODA. The solid line represents a least squares fit that corresponds to 5.2% charged (protonated) ODA groups. (f) The stability of QDs functionalized with 25 mol% ODA versus time.

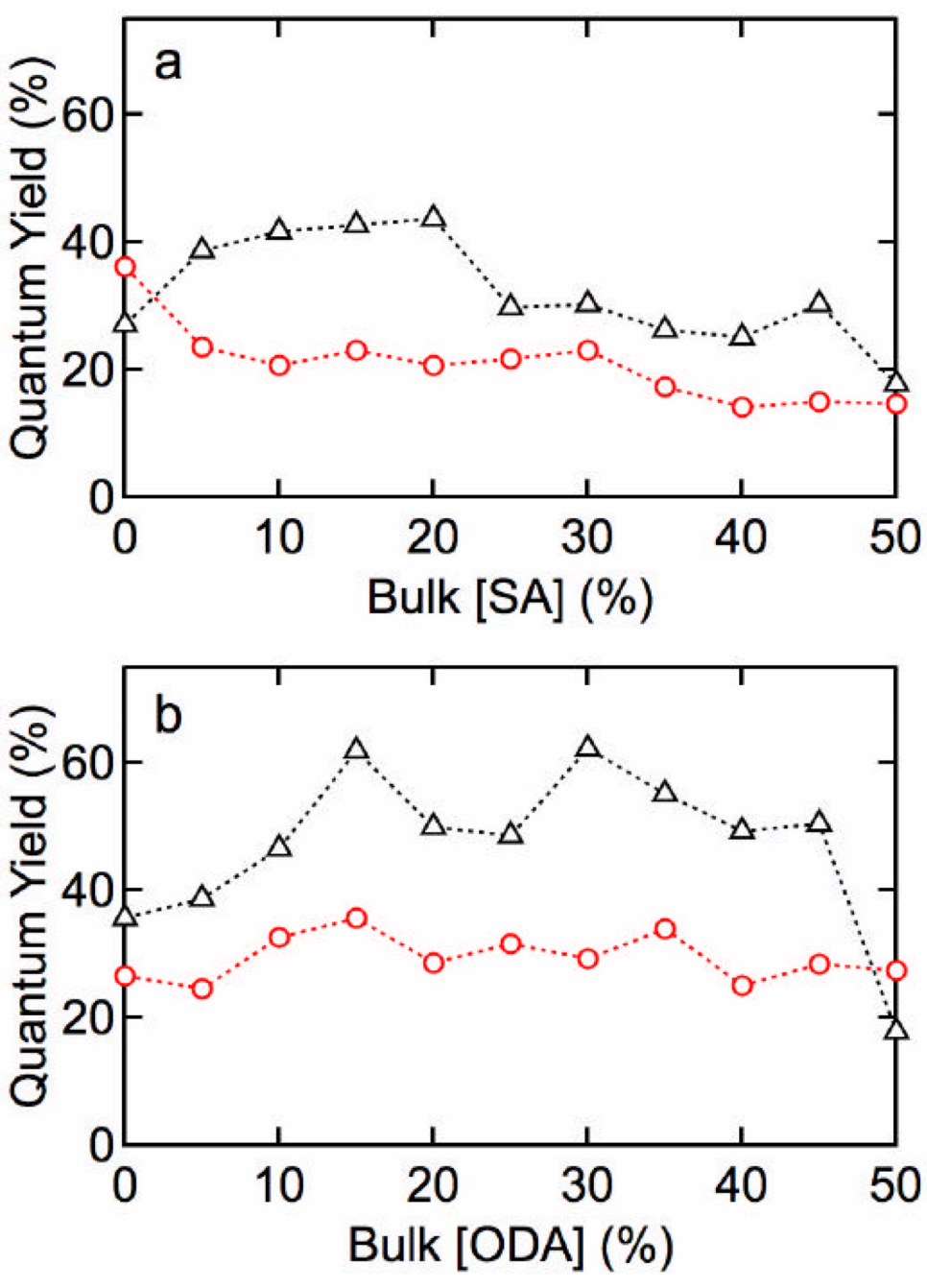

Figure 3.
Quantum yield for QDs water solubilized with (a) SA/MHPC or (b) ODA/MHPC. (?) thiolated and (o) unthiolated QDs.

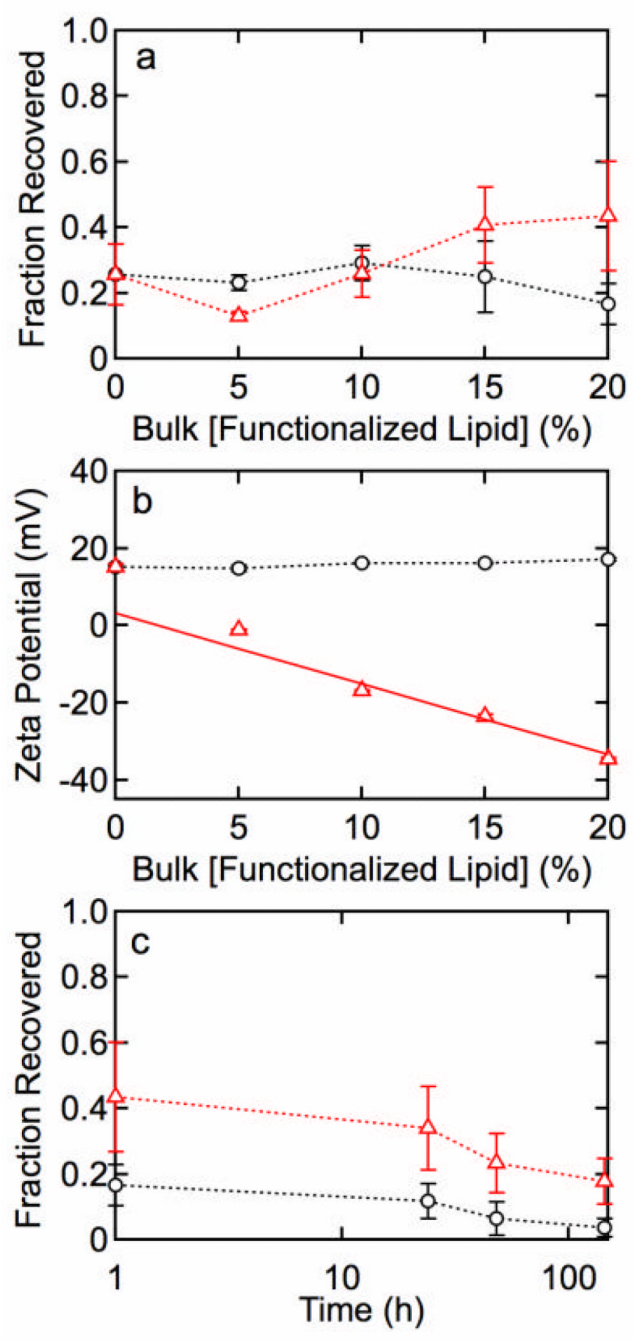

Figure 4.

(a) Fraction of QDs recovered after water solubilization with 80 mol% MHPC, 20 – × mol% DPPE, and (?) × mol% DPPE-COOH or (o) × mol% DPPE-NH_2. (b) Zeta potential versus concentration of (?) DPPE-COOH or (o) DPPE-NH_2. The solid line represents a least squares fit that corresponds to 12.3% charged (deprotonated) DPPE-COOH groups. (c) Fraction of QDs recovered versus time demonstrating a lack of stability for 20 mol% (?) DPPE-COOH and (o) DPPE-NH_2. The fraction recovered for QDs functionalized with DPPE-COOH is significantly higher than QDs functionalized with DPPE-NH_2.

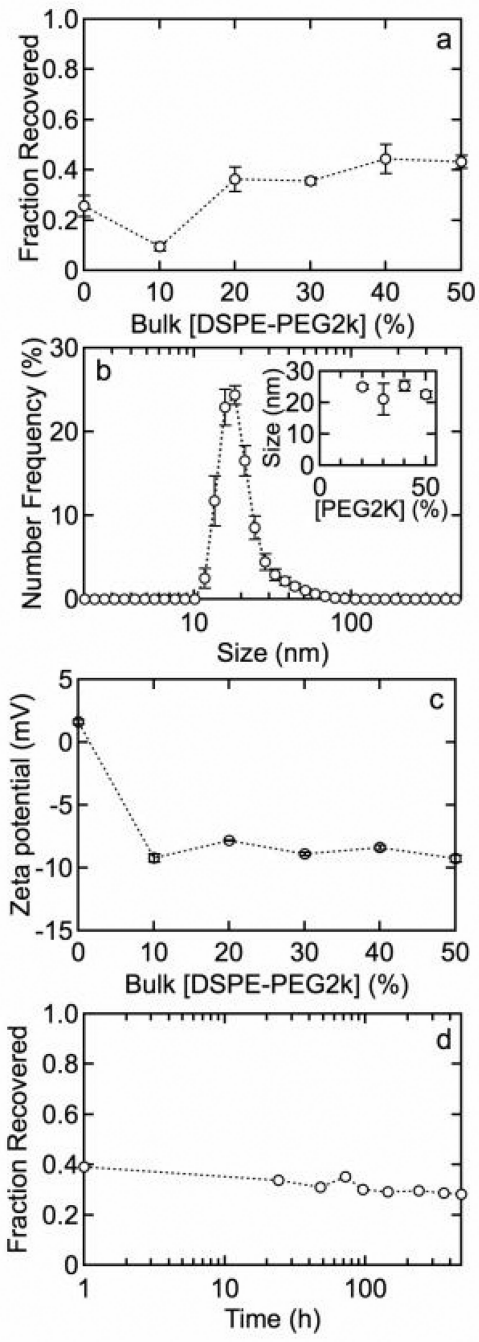

Figure 5.

(a) Fraction of QDs recovered 30 min after water solubilization versus DSPE-PEG2k concentration with MHPC. After 20 mole% DSPE-PEG2k the fraction recovered reaches a plateau. (b) Particle size distributions for QDs with 20 mol% DPSE-PEG2k. The average size was 20.5 ± 0.9 nm. The inset shows the average size versus mol% DSPE-PEG2k. (c) Zeta potential versus concentration of DSPE-PEG2k in solution showing that PEG creates a slightly negative colloid. (d) Fraction of QDs recovered versus time for QDs functionalized with 20 mol% DSPE-PEG2k. Only a slight drop in stability is observed after 500 h.

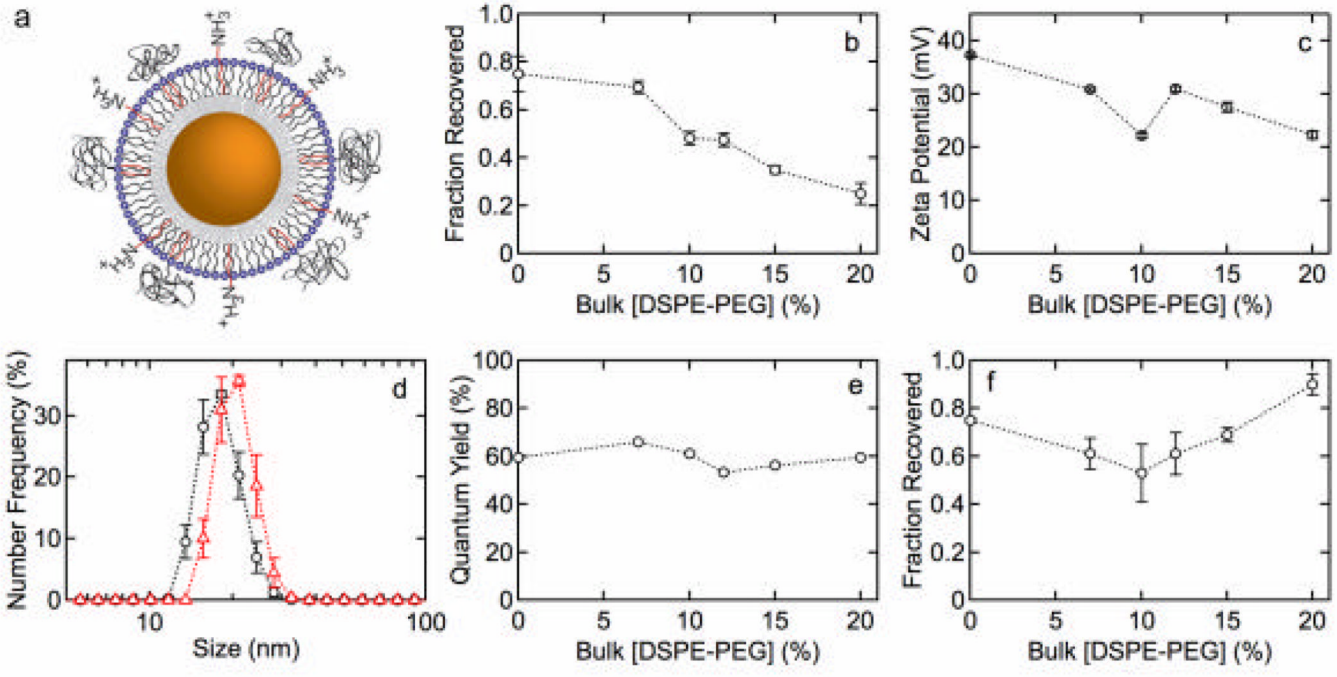

Figure 6.

(a) QD lipid functionalization scheme: 1-dodecanethiol inner leaflet and an ODA/MHPC/DSPE-PEG2k outer leaflet. The concentration of ODA was fixed at 30 mol%. (b) Fraction of QDs recovered versus concentration of DSPE-PEG2k. (c) Zeta potential versus concentration of DSPE-PEG2k. (d) Size distributions for QDs with (o) 10 mol% and (?) 20 mol% DSPE-PEG2k. The average sizes are 16.0 ± 0.5 and 17.8 ± 0.6 nm, respectively. (e) QY versus concentration of DSPE-PEG2k. (f) Fraction of QDs recovered versus concentration of DSPE-PEG2k after incubation in 100 mM phosphate buffer for 1 h.

Table 1

Summary of lipid compositions studied. ODA - octadecylamine, SA – stearic acid, DDT – dodecanethiol, HDA - hexadecylamine, TOPO - trioctylphosphine oxide, MHPC - 1-myristoyl-2-hydroxy-sn-glycero-3-phosphocholine, DPPE - 1,2-dipalmitoyl-sn-glycero-3-phosphoethanolamine, DPPE-COOH - 1,2-dipalmitoyl-*sn*-glycero-3-phosphoethanolamine-N-(lauroyl), DPPE-NH_2 - 1,2-dipalmitoyl-sn-glycero-3-phosphoethanolamine-N-(lauroylamine).

Inner Leaflet	Outer Leaflet	Comments
HDA/TOPO	MHPC + SA	• zeta potential decreases with increasing [SA] • excellent stability with time • maximum stability > 20 mol% SA
HDA/TOPO	MHPC + ODA	• zeta potential increases with increasing [ODA] • excellent stability with time • maximum stability > 20 mol% ODA
DDT	MHPC + SA	• zeta potential decreases with increasing [SA] • excellent stability with time • maximum stability > 20 mol% SA • high QY
DDT	MHPC + ODA	• zeta potential increases up to 30 mol% ODA • good stability with time • maximum stability > 20 mol% ODA • highest QY
HDA/TOPO	MHPC + DSPE or DPPE	• zeta potential constant with increasing [DSPE] • low stability with time • maximum stability at 20 mol% DSPE
HDA/TOPO	MHPC + DPPE-COOH	• zeta potential decreases with increasing [DSPE-COOH] • low stability with time • maximum stability at 15 mol% DPPE-COOH
HDA/TOPO	MHPC + DPPE-NH_2	• zeta potential constant with increasing [DSPE-NH_2] • low stability with time • maximum stability at 10 mol% DPPE-NH_2
HDA/TOPO	MHPC + DSPE-PEG2k	• zeta potential constant with increasing [DSPE-PEG2k] • low stability with time maximum stability at 20 mol% [DSPE-PEG2k]
DDT	MHPC + DSPE-PEG2k & ODA	• zeta potential decreases with increasing [DSPE-PEG2k] fixed [ODA] • good stability in buffer • maximum stability at 7 mol% [DSPE-PEG2k]